Published in final edited form as:
J Propuls Power. 2018 March ; 34(2): 438–448. doi:10.2514/1.B36550.

Development of a Premixed Combustion Capability for Dual-Mode Scramjet Experiments

Robert D. Rockwell[1], **Christopher P. Goyne**[2], **Harsha Chelliah**[3], **James C. McDaniel**[4], **Brian E. Rice**[5], **Jack R. Edwards**[6], **Luca M. L. Cantu**[7], **Emanuela C. A. Gallo**[8], **Andrew D. Cutler**[9], **Paul M. Danehy**[10]

[1]Senior Scientist, Mechanical and Aerospace Engineering, Member AIAA. University of Virginia, Charlottesville, Virginia 22904

[2]Associate Professor, Mechanical and Aerospace Engineering, Associate Fellow AIAA. University of Virginia, Charlottesville, Virginia 22904

[3]Professor, Mechanical and Aerospace Engineering, Associate Fellow AIAA. University of Virginia, Charlottesville, Virginia 22904

[4]Professor, Mechanical and Aerospace Engineering, Associate Fellow AIAA. University of Virginia, Charlottesville, Virginia 22904

[5]Research Aerospace Engineer, High Speed Systems Division, Member AIAA. U.S. Air Force Research Laboratory, Arnold Air Force Base, Tennessee 37389

[6]Professor, Mechanical and Aerospace Engineering, Associate Fellow AIAA. North Carolina State University, Raleigh, NC 27695

[7]Ph.D. Candidate, Mechanical and Aerospace Engineering, Member AIAA, The George Washington University, Washington, DC 20052

[8]Ph.D. Candidate, Mechanical and Aerospace Engineering, Member AIAA, The George Washington University, Washington, DC 20052

[9]Professor, Mechanical and Aerospace Engineering, Associate Fellow AIAA. The George Washington University, Washington, DC 20052

[10]Research Scientist, Advanced Measurements and Data Systems Branch, Associate Fellow AIAA. NASA Langley Research Center, Hampton, VA 23681

Abstract

Hypersonic air-breathing engines rely on scramjet combustion processes, which involve high-speed, compressible, and highly turbulent reacting flows. The combustion environment and the turbulent flames at the heart of these engines are difficult to simulate and study in the laboratory under well controlled conditions. Typically, wind-tunnel testing is performed that more closely approximates engine development rather than a careful investigation of the underlying physics that drives the combustion process. The experiments described in this paper, along with companion data sets, aim to isolate the chemical kinetic effects and turbulence-chemistry interaction from the fuel-air mixing process in a dual-mode scramjet combustion environment. A unique fuel injection approach is adopted that produces a uniform fuel-air mixture at the entrance to the combustor and results in premixed combustion. This approach relies on the mixing enhancement of a

precombustion shock train upstream of the dual-mode scramjet's combustor. For the first time a stable flame, anchored on a cavity flameholder, is reported for a scramjet combustor operating in premixed fuel-air mode. The new experimental capability has enabled numerous companion studies involving advanced diagnostics such as coherent anti-Stokes Raman scattering (CARS), particle image velocimetry (PIV), and planar laser induced fluorescence (PLIF).

I. Introduction

Sustained hypersonic flight via scramjet propulsion presents considerable capabilities for future space access and high-speed weapons. However, in order for this technology to become a practical and reliable propulsion method, there is a need for improved understanding and prediction of the reacting flow of the scramjet combustor, which is highly compressible and highly turbulent. The fundamental processes in the combustor include the injection, mixing, and reaction of a fuel in a high-speed airstream. For certain fuels, such as hydrogen, the chemical kinetic time scales are much shorter than the flow time scales. Hence flame stabilization is primarily controlled by fuel-air mixing. While hydrocarbon fuels have longer kinetic time scales than hydrogen, a stable flame can be realized if the local static temperature is high enough or if a flameholder is present and an adequate source of combustion radicals is generated in the vicinity of the flameholder. In order to focus on a process that is fundamental to flame stabilization in scramjet engines, the present study examines high-speed premixed fuel-air flows. In this way, the fuel-air pre-mixing can be decoupled from the turbulent chemistry interactions occurring in the flame stabilization region. Models of turbulence-chemistry closures can then be developed and validated. Investigations of the effect of turbulent fluctuations on flame structure, including eddy sizes and distributions, can also be conducted. Furthermore, complications, such as the effect of jet mixing on flame propagation, can be avoided.

Unlike in non-premixed turbulent combustion, where there is no meaningful time scale based on velocity, in premixed turbulent combustion the velocity fluctuations, v', play a critical role in defining the turbulent combustion regimes. For low density ratio variations, the dependence of normalized turbulent velocity fluctuations with respect to laminar burning velocity, v'/s_L, to the normalized integral turbulent length, l/l_L are well established, and are given by

$$\begin{aligned} \frac{v'}{s_L} &= Re_l\left(\frac{l}{l_L}\right)^{-1}, \\ &= Da_l^{-1}\left(\frac{l}{l_L}\right), \\ &= Ka_\eta^{2/3}\left(\frac{l}{l_L}\right)^{1/3}, \end{aligned} \tag{1}$$

where Re_l is the Reynolds number based on integral length scale, Da_l is the Damkohler number based on integral length scale, and Ka_η is the Karlovitz number based on Kolmogorov length scale [1]. For large Re_l numbers, the above relationships yield four distinct turbulent combustion regimes identified as wrinkled flamelets, corrugated flamelets, distributed reaction zones, and well-stirred reaction zones [2]. It is currently not known in

which regime a scramjet with premixed combustion operates. Therefore, a high-speed premixed combustion capability is desirable in order to conduct experiments to identify the combustion regime of these flames.

For scramjet combustion that involves turbulent compressible reacting flows with large density variations, the turbulent combustion regimes are influenced by an additional parameter, S, characterized by

$$S = \Delta T_s / \Delta T_c, \tag{2}$$

where ΔT_s is the change in temperature associated with kinetic energy and ΔT_c is the change in temperature associated with the chemistry [3]. If the rise in temperature associated with kinetic energy is approximated by

$$\Delta T_s = \frac{1}{2}(\gamma - 1) M^2 T_0, \tag{3}$$

then the parameter S becomes

$$\mathrm{S} = \frac{1}{2}(\gamma - 1) M^2 \frac{T_0}{\Delta T_c}. \tag{4}$$

Here, γ is the specific heat ratio, M is Mach number, T_0 is static temperature, and $\Delta T_c / T_0$ can be identified as a heat release parameter, α, with typical values ranging from 1 to 10 [4]. If typical values of $\alpha = 6$ and $\gamma = 1.33$ are selected, then M = 6 flow yields $S = 1$, indicating that velocity fluctuations can lead to temperature fluctuations of the same order as the temperature increase by chemical reactions. This demonstrates how closely coupled velocity fluctuations and chemical reactions can be in the high-speed combustion environment of a scramjet. By decoupling the mixing from the turbulent combustion process, the experiments described in this paper offer an opportunity to examine the turbulence-chemistry coupling in a scramjet relevant environment.

Therefore, the main goal of the present research is to develop a high-speed premixed combustion capability to enable investigation of the strong coupling between flow compressibility, turbulence, and heat release. By applying advanced diagnostics, the exact turbulent combustion regime of the scramjet combustor may be identified. Such measurements have not been previously published for scramjet combustors nor has stable, high-speed, premixed combustion been demonstrated. The specific objectives of the present study are to: 1) design and construct fuel-air premix hardware for a series of high-speed combustion experiments, 2) demonstrate stable premixed combustion in a scramjet combustor, and 3) examine the effects of fuel equivalence ratio and inflow gas temperature on flame ignition, propagation, and flameout. The application of advanced optical diagnostics and the identification of the turbulent combustion regime is examined in companion studies (as discussed below).

A typical hydrocarbon-fueled scramjet engine utilizes one or more sidewall cavity flameholders, which provide a region of hot recirculating flow adjacent to the main scramjet

flowpath. The cavity serves to increase fuel residence time and provides a source of combustion radicals to the freestream [5–7]. Fuel is often introduced directly into the cavity through the base or closeout wall, or injected immediately upstream to seed the shear layer between the cavity and freestream [8–10]. With either approach, the freestream and fuel at the entrance to the combustor, defined for these purposes as the leading edge of the cavity, are not premixed. Thus, mixing and combustion occur concurrently in the combustor within and downstream of the cavity.

Alternatively, premixed combustion requires that fuel be introduced into the airflow well upstream of the combustor, such that there is ample time and distance for mixing of the fuel and air streams to take place. This approach has been considered since the early days of scramjet engine design and addresses several significant challenges of the scramjet combustion process [11]. In particular, upstream fuel injection provides additional time and duct length for mixing of the fuel and air. Also, the inlet and isolator of a scramjet vehicle are likely to contain shocks or shock systems, including bow shocks from the aircraft forebody and inlet, and an oblique or normal precombustion shock train in the isolator. Several studies have demonstrated enhanced mixing of fuel jets when processed by such shocks or shock systems [8, 12–15]. The added length and exposure to an inlet or isolator shock system may also provide additional breakdown of fuel droplets and cracking of hydrocarbon fuels [16].

Unfortunately, upstream fuel injection in a scramjet can be associated with several challenges. First, there is the potential for premature ignition of the fuel, most likely in the hot boundary layer, which can lead to isolator or inlet flashback [17]. Further, flow blockage associated with upstream fuel injectors can cause a loss of total pressure with a subsequent drop in engine thrust generation [18–19]. Finally, flashback and blockage, either alone or in concert, have the potential to unstart the inlet with a corresponding loss of air flow through the engine [17].

Numerous upstream fuel injection mechanisms and geometries have been proposed and studied through the years as researchers search for the optimal combination of operational benefit and risk mitigation. These include normal and angled injection directly into the supersonic flow from flush wall injectors as well as from or behind various types of struts, pylons, and ramps [17, 20–24]. A concept developed at the University of Queensland is that of radical farming where small pockets of limited combustion within the inlet’s oblique shock system produce radicals that are then available for initiation of more vigorous combustion downstream [25]. These processes have been verified and evaluated experimentally and numerically for enthalpies at equivalent flight Mach numbers of 8 to 12 [26–27].

One of the primary mechanisms for shock-induced mixing enhancement is the baroclinic vortex generation that occurs in regions where pressure and density gradients are misaligned [28]. This may occur in a scramjet inlet at the interface between fuel and air streams passing through a shock [29–30]. In the late 1980’s, Marble et al. proposed a unique type of scramjet fuel injector that was specifically designed to take advantage of baroclinic vortex generation as a means of enhancing fuel-air mixing upstream of the combustor [31]. The design

involved several ramp fuel injectors in a contoured wall cavity that directed the fuel streams into an oblique shock generated immediately behind the injectors. Follow-on experimental and numerical studies demonstrated the effectiveness of this design [32–33].

Upstream fuel injection is potentially very useful in the case of a dual-mode scramjet with flight Mach numbers in the range of 4 to 6 where a theoretical flight vehicle would be expected to transition from a subsonic ramjet mode of combustion to a supersonic scramjet mode of combustion. The relatively lower enthalpies in this flight regime may reduce the risk of isolator flashback or boundary layer ignition due to lower static temperatures in the boundary layer, typically on the order of 950 to 1500 K. Furthermore, the isolator of a dual-mode scramjet typically contains a precombustion shock train, which diminishes in strength with increasing inlet Mach number. Taking advantage of the mixing enhancement provided by this naturally occurring shock train could result in a reduced total isolator/combustor length with a commensurate space and weight savings. The approach taken in this study is to inject fuel from multiple ports at the upstream end of the isolator with low dynamic pressure relative to the freestream. This technique minimizes disruption of the incoming freestream by the fuel injectors themselves and relies on mixing through the precombustion shock train to produce a uniform fuel-air mixture at the combustor entrance.

This study was part of a larger effort of the National Center for Hypersonic Combined Cycle Propulsion (NCHCCP) aimed at examining combustion in a dual-mode scramjet. As part of this larger effort, a suite of advanced instream diagnostics were available including coherent anti-Stokes Raman scattering (CARS), OH and CH_2O planar laser induced fluorescence (PLIF), and particle image velocimetry (PIV) [34–36]. Together with conventional measurement techniques, these diagnostics enabled the study of both the cavity flow (operability limits, residence time, internal cavity flame structure, and shear layer characterization) and the main flame (flame surface area, local strain rate/stretch and flame propagation angle). The experiments described in this paper have resulted in CARS, PLIF, and PIV databases and, through collaboration with the NCHCCP, validation of advanced time averaged and time accurate numerical models [37]. The purpose of this paper is to report on the development and demonstration of the premixed capability and the initial experimental results.

This paper first presents the experimental approach followed by a description of the facility and experimental test conditions. Details of the fuel injection and mixing processes are then discussed and the fully premixed nature of the combustor inflow is established. Finally, combustion characteristics for the premixed dual-mode scramjet are presented including static wall pressure traces, integrated combustor pressure forces, and operability limits, along with high-speed chemiluminescence images of the premixed flame. In order to provide appropriate detail and context for the experimental to numerical comparison, the present paper serves to fully describe the experiment and diagnostics that are not detailed elsewhere. In addition, this paper documents the first demonstration of a cavity stabilized flame in a scramjet combustor operating in premixed fuel-air mode. A particularly novel aspect of the adopted approach is that the combustion-backpressured shock train in the scramjet isolator is used to premix the fuel and air upstream of the combustor.

II. Experimental Approach

The dual-mode scramjet experiments were conducted with the aim of examining the flow processes that take place in the isolator and combustor in the flight Mach number regime of 4 to 6. Specifically, the experiments employ a direct-connect scramjet combustor that is operated at Mach 5 enthalpy (total temperature of 1200 K) using the University of Virginia Supersonic Combustion Facility (UVaSCF). The test-section hardware has been designed to accommodate the application of multiple advanced flow diagnostic techniques [38]. In particular, the combustor section incorporates a modular construction approach that provides substantial access for optical laser diagnostics. In addition to static wall pressure and temperature measurements, a number of advanced, instream diagnostics have been applied in the facility, including CARS, OH PLIF (Hz), CH_2O PLIF (Hz and kHz), NO PLIF (Hz), stereoscopic and planar PIV (Hz and kHz), and high-speed chemiluminescence imaging (kHz). Combined, these diagnostics result in the measurement of: wall static pressure, temperature, fuel distribution, species concentration (N_2, O_2, H_2, CO, CO_2, H_2O, C_2H_4, and qualitative OH and CH_2O), scalar correlations, three-component velocity, three-component turbulence intensity (RMS), and Reynolds stresses.

The experiments described in this paper have used ethylene fueling in what is termed the modified Configuration E (Fig. 1). The flowpath starts with a Mach 2 facility nozzle and incorporates a long, constant-area isolator upstream of the combustor that contains any precombustion shock train. Injecting fuel at the upstream end of the isolator allows for significant mixing of the fuel into the freestream ahead of the cavity flameholder. The isolator is a 484.96 mm long rectangular duct with a 25.4 mm by 38.1 mm cross-section. A 2.9° divergence on the cavity-side wall starts 53.44 mm upstream of the cavity leading edge. This divergence is maintained through the combustor and extender sections of the flowpath. A constant-area section downstream of the combustor compresses the flow and induces a thermal throat when the flowpath is operating in the dual-mode. This results in a precombustion shock train in the isolator and subsonic flow through the combustor. The cavity spans the width of the duct and has an initial depth of 9.04 mm, which is maintained over a length of 31.04 mm. The cavity closes with a 22.5° ramp that ends 53.35 mm downstream of the leading edge. The scramjet flowpath terminates with an atmospheric backpressure at the exit, 497.99 mm downstream of the cavity leading edge. The scramjet exit is 1.036 m from the exit of the Mach 2 nozzle.

All components in the flowpath were constructed of stainless steel with the exception of the cavity wall of the combustor, which is OFHC copper, and the large optical windows in the combustor, which are 9.53 mm thick fused silica. Water cooling is incorporated in each component of the test-section and all stainless steel walls in the isolator, combustor, and constant area section are coated with a 0.381 mm thick layer of thermal barrier zirconia. The copper cavity wall is not coated.

The primary measurement locations are indicated in Fig. 1. Nitric oxide (NO) PLIF measurements were taken on a transverse plane at the leading edge of the cavity to verify the level of premixing. Other measurements taken in this flowpath but not reported here include CARS, PLIF (OH and CH_2O), and PIV. The vertical dotted lines in Fig. 1 represent the

CARS measurement locations. Normalized by the cavity depth (h = 9.04 mm), these measurement planes are at axial locations of x/h = −9.14, 2.39, 6.60, and 10.80 relative to the cavity leading edge. PLIF (OH and CH_2O) has been performed from the cavity leading edge to the downstream end of the optical windows in the duct, as indicated by the dashed box in Fig. 1. The cavity-side wall is instrumented from inlet to exit with 80 low frequency pressure taps and 13 type K thermocouples located on the combustor centerline.

III. Facility and Flow Conditions

The UVaSCF is an electrically heated, continuous flow, direct-connect scramjet wind tunnel. It is capable of simulating up to Mach 5 flight enthalpy and provides a clean test flow that is free of contaminates such as those from a vitiation heater. Facility run times are on the order of hours with steady-state heating and fuel conditions. Because CARS is a point-by-point measurement technique, the long duration experimental run times provide for high spatial resolutions using a finely-spaced measurement grid [34]. Likewise, PIV and PLIF require non-correlated image counts on the order of 1000 to 2000 or more for calculating average turbulence statistics and other parameters to a reasonable degree of statistical convergence [36, 39–40]. Coupled with the optical access in the tunnel and proximity to laser diagnostics labs, the facility is well suited to the application of these advanced optical diagnostic techniques.

The facility flow conditions are presented in Table 1. The uncertainties given in the table are calculated by standard propagation of error and include temporal variability as well as instrumentation uncertainty. Tunnel air flow conditions are typically maintained to less than ±1% during a run and across multiple runs. The facility is fully described elsewhere [41–43].

As shown in Fig. 1, an air throttle is available downstream of the combustor, near the upstream end of the extender (at x/h = 37.52). This allows the duct to be back pressured in conjunction with a combustion process or independently to simulate the pressure rise associated with combustion in a nonreacting flow. The throttle consists of two slotted, high pressure air injectors, one in each side wall, that are used to restrict flow at that location. The slots are 3.175 mm wide and extend over the full height of the duct. Through use of the air throttle, it is possible to accurately locate and stabilize the leading edge of the isolator shock train at any point in the duct. Although air throttle pressures and flow rates are not generally measured directly, the isolator pressures were monitored in real time with adjustments made to the throttle to maintain the desired shock location.

A NetScanner™ pressure scanner and remote NetScanner™ thermocouple unit were used to acquire wall pressures and temperatures along the centerline of the cavity-side wall in the scramjet flowpath. Typically, a scan of 20 samples was acquired over 2 seconds at a sample rate of 10 Hz for each pressure tap and thermocouple. This data was then averaged and normalized by the measured pressure at the most upstream pressure tap (located 6.35 mm downstream of the facility nozzle exit) prior to plotting. Wall pressures and temperatures were typically measured to within ±0.5% and average quantities had a 95% confidence interval of no more than ±1.5%.

IV. Fuel Injection and Mixing

The primary objective for the fuel injection scheme developed in this work was to generate a premixed flow of ethylene fuel and air across the duct at the combustor entrance. The combustor entrance was defined as the leading edge of the cavity for the purposes of this study. It was expected that placing the fuel injectors close to the exit of the facility nozzle, well upstream of the cavity flameholder, would allow the maximum time and distance for fuel-air mixing in the isolator. Although introducing fuel into the isolator carries the risk of the flame flashing forward of the combustor, it was not known at the outset whether this would be a controllable phenomenon or what the repercussions for the facility would be.

In order to maximize mixing efficiency, several fueling strategies were considered including injection through a single row of injectors distributed laterally across the duct, staged injection through two or more closely-spaced rows of injectors, and angled injection at 30 or 45 degrees. In addition to the level of mixing, a tradeoff to be considered was the potential for blockage of the freestream air flow, which could unstart the facility nozzle.

Three sonic fuel injectors per row, each with a diameter of 1.245 mm produced a reasonable mechanical design for the facility. A single row of injectors can deliver sufficient fuel for a global equivalence ratio, ϕ, of 0.75 at a total pressure of about 1900 kPa, which is the limit for existing upstream components in the fuel system. Table 2 lists several potential combinations of fuel injectors available at each injector bank in the facility along with the estimated fuel dynamic pressure, Q, and fuel-to-freestream dynamic pressure ratio for each injector. While the table assumes a nominal discharge coefficient of 0.6 for each row of injectors, measurements on the fabricated hardware revealed a variation between 0.56 and 0.66 for the individual rows. There are a total of four injector banks available in the isolator hardware of the facility located at the upstream and downstream ends of the isolator, on the cavity-side and opposite-side walls. Only the upstream banks were used for the experiments described in this paper.

Figure 2 shows results from a RANS CFD study of several potential fueling strategies based on fuel injection from the cavity-side wall at the upstream end of the isolator [44]. Asymmetries in the crossplanes are due to an assumption of nonuniform total temperature at the inflow plane, which is consistent with previous CARS measurements in the facility [34,37,45]. In all cases, the total amount of fuel being injected produces a global equivalence ratio of 0.5 and the mass flow of fuel through each injector is assumed to be identical. Thus, with two-rowed injection (90/90, 45/90, or 30/45), the mass flow and dynamic pressure of fuel injected through any one injector are half of what they would be in the case of single-row injection (90, 45, or 30). The numbers in the left hand column refers to the angle of fuel injection with respect to the incoming air flow. The crossplane images in Fig. 2 show that the use of normal injection, either through two closely spaced rows or a single row, produces the most uniform distribution of fuel in the cavity with a local equivalence ratio of about 1 in the middle of the cavity. The cases with angled injection produced highly nonuniform mixtures in the cavity due to the production of strong vortices, which lift the fuel plume away from the wall and allow clean air to penetrate underneath.

While recognizing that RANS results may not be the best predictor of turbulent mixing, a decision was made to focus on the normal fuel injectors based on the results shown in Fig. 2. Further, two-rowed injection was chosen as the primary injection scheme over single-rowed injection because it requires lower fuel pressures to deliver the same amount of fuel while producing a nearly identical mixing profile in the cavity. This decision is also consistent with the studies in Ref. 19, which found that dual-staged normal injection provides significantly enhanced mixing over a single injector, but also highlighted the importance of minimizing the dynamic pressure ratio in order to reduce the stagnation pressure loss. Finally, in these simulations fuel is only able to penetrate about halfway across the duct, regardless of the injection scheme. From these results it was clear that producing a uniform mixture across the duct would require additional fuel injectors on the opposite wall and additional mixing, such as could be achieved using the precombustion shock train.

Figure 3 shows results from a similar RANS CFD study looking at the effect of a shock train in the isolator on free stream fuel-air mixing. Here, the global equivalence ratio was set at 0.35, which, as will be discussed later, is close to the lean flame out limit for this flowpath with fully premixed fueling, and the backpressure at the combustor exit was increased such that the leading edge of the isolator shock train was located at $x/h = -54$, immediately downstream of the fuel injector location. Fuel injection is through two rows of normal injectors on the cavity-side wall. The shock train clearly enhances the fuel-air mixing process leading to a decreased local equivalence ratio in the cavity (~0.55 vs. 0.9 in the non-backpressured case) and more uniform fueling across the duct. As above, asymmetries in the cross-stream mixing are due to a nonuniform total temperature distribution at the inflow plane resulting in an asymmetric shock train.

From these numerical studies it was determined that achieving a uniformly premixed flow at the cavity entrance plane would be possible by using a combination of distributed fuel injection at the upstream end of the isolator from both the cavity-side and opposite-side walls of the duct along with the mixing enhancement of a sufficiently long precombustion shock train. Thus, as indicated in Fig. 1b, the primary ethylene fuel injection is through two banks of six sonic, flush-wall injectors located at the upstream end of the isolator, 38.1 mm downstream of the facility nozzle exit on opposite walls of the duct. Injection at this location allows the fuel to be processed by the isolator shock train, ideally resulting in a fully premixed flow at the cavity leading edge. Each bank comprises two rows of three equally spaced 1.245 mm diameter injectors oriented normal to the freestream flow. The total fuel pressure and temperature for each set of injectors is monitored and controlled to provide the desired fuel split and flow rate.

Table 3 lists the primary fueling conditions used in these experiments. As will be discussed later, the first fuel condition represents the maximum fuel rate that can be accommodated by the flowpath without risking the shock train impinging on the fuel injectors. The second fuel condition is close to the lean flameout point of the flowpath with a fully premixed combustor inflow. There is a difference in the fuel injection pressures between the cavity-side bank and the opposite-side bank, which is due to a small difference in the discharge coefficients of the two injector banks (0.60 for the cavity-side bank and 0.56 for the opposite-side bank). Control valves in the fuel system allow the fuel to be evenly split between the two injector

banks as shown in Table 3 or adjusted such that a larger proportion of fuel is delivered through the cavity-side injector bank. As before, the uncertainties given in the table reflect instrumentation uncertainty as well as temporal variability of the facility during a single run or across multiple runs. For any specific measurement, such as a single pressure scan or flameout test, the uncertainty in equivalence ratio is ±2.6%.

Ethylene typically does not autoignite in this flowpath at the conditions of interest. However, following an ignition procedure, the flame is self-sustaining. Ignition was achieved by using the air throttle to pressurize the cavity while injecting a small amount of hydrogen through a port in the base of the cavity. Under these conditions the hydrogen autoignites and ethylene fuel can then be introduced through the upstream injectors. Once a sufficient flow rate of ethylene is established (typically a global fuel equivalence ratio greater than 0.33), the hydrogen can be turned off. The air throttle may be maintained or not depending on the nature of the particular experiment being performed.

NO PLIF measurements were used to experimentally evaluate the level of fuel premixing at the leading edge of the cavity. A mixture of 10% (molar) NO in nitrogen was used as a surrogate for the ethylene fuel and a nonreacting mixing study was performed. Importantly, the molar weight of this NO/N_2 gas mixture is nearly identical to that of ethylene, which allows the fuel system operation, including injection pressures, to be the same for equivalent mass flow rates of NO and ethylene. With no combustion process present, the air throttle was used to generate a combustor back pressure equivalent to that due to combustion at a given fuel equivalence ratio and thus drive the isolator shock train. A full description of the NO PLIF measurements is given elsewhere [40].

Uniform fuel premixing for the case with both banks of isolator injectors operating and a precombustion shock train in the isolator has been confirmed with the NO PLIF as shown in Figs. 4 and 5. Figs. 4a and 5a are single-shot instantaneous images and Figs. 4b and 5b show the average distribution for simulated global equivalence ratios of 0.44 and 0.35 respectively, which correspond to the operating conditions discussed above. These images present a qualitative representation of the fuel distribution at the cavity leading edge. Taking into account some of the image artifacts, such as a left to right variation due to attenuation of the laser sheet as laser light is absorbed by the NO molecules, the measurements show an essentially uniform fuel-air mix. Further analysis of the NO PLIF images produced an estimated mixing efficiency of approximately 90% for each of these cases [40]. For comparison, Fig. 6 shows the fuel distribution from a single isolator fuel injector located on the centerline of the cavity-side wall with no shock train to promote mixing. In this case, the dark region along the lateral edges and on the wall opposite the active fuel injector shows that NO has not propagated to fill the duct and the mixing efficiency is approximately 24% [40].

V. Results

The primary results discussed here are the static wall pressures measured along the length of the flowpath on the cavity-side wall and the operability limits of the flowpath in which sustained premixed ethylene combustion is possible. These results demonstrate stable

flameholding in premixed mode and establish the operating envelope and flow conditions for further experimental studies. CARS and OH PLIF measurements have been reported separately [46–48]. These papers present and compare spatially and temporally resolved temperatures, species concentrations, and estimations of flame location and flame angle between measurement techniques as well as with LES/RANS numerical simulations [44]. In summary, the measurements reflect a highly turbulent, unsteady flame propagating downstream from the cavity with a flame angle of approximately 10°.

Figures 7 and 8 show the axial distribution of static pressure on the cavity-side wall for global fuel equivalence ratios, ϕ, of approximately 0.40 and 0.34, respectively. The measured pressures have been normalized by the static pressure at the exit of the facility nozzle, P_{ref}, and the axial locations are normalized by the cavity depth, h. The cavity leading edge is at x/h = 0. Results for the case with fuel being delivered equally from both sides of the isolator are shown as solid square symbols. This fueling scenario is equivalent to that shown in Figs. 4 and 5 and represents the uniform fuel-air premix case. Two additional fuel split ratios are included for comparison. The open symbols represent a fuel split with approximately twice as much fuel injected from the cavity-side wall as the opposite wall and the crossed symbols represent fuel injection from the cavity-side wall only. This last condition is similar to the RANS CFD study shown in Fig. 3. Although mitigated somewhat by the presence of an isolator shock train, delivering all of the fuel through the cavity-side injectors alone results in some level of fuel stratification with a higher fuel density on the cavity side of the duct (see Fig. 3). All fuel conditions shown in Figs. 7 and 8 produce a stable dual-mode scramjet flame anchored on the cavity that can be maintained for one to two hours in the facility with depletion of the fuel tanks being the limiting factor.

Also shown in Figs. 7 and 8 are the pressure distributions for the NO PLIF measurements, represented by a dashed line. In these cases the air throttle rather than a combustion process was used to generate the back pressure that drives the shock train in the isolator. The pressure rise in the isolator is the same whether it is due to a combustion process or the air throttle giving confidence in the NO PLIF mixing study. The fuel off case is included for reference.

Fig. 7 shows that at global fuel equivalence ratios above 0.4, the leading edge of the precombustion shock train is approaching the isolator fuel injection location. Care must be taken during these experiments to avoid impingement of the shock train directly on the fuel injectors as that results in ignition of the fuel in the isolator leading to a large pressure spike in the flowpath and likely damage or breakage of the windows. Thus, to provide some operating margin and avoid damaging tunnel hardware, a practical upper fueling limit for continuous testing is a global equivalence ratio of 0.42 with an absolute upper bound of 0.45. Likewise, Fig. 8 depicts a practical lower equivalence ratio limit for fully premixed ethylene fueling. As discussed later, at global equivalence ratios approaching 0.3, the local equivalence ratio in the cavity is too low for sustained ethylene combustion.

All of the fueled cases shown in Figs. 7 and 8 represent operation of the scramjet flowpath in the dual-mode with separated flow and a precombustion shock train in the isolator. Using a one-dimensional model of the separated flow in the isolator [49], the one-dimensional Mach

number in the core flow at the cavity leading edge is estimated to be 0.70 for the $\varphi = 0.40$ case and 0.73 for the $\varphi = 0.34$ case. A thermal throat is observed at the downstream end of the constant area section (x/h = 35), which represents the transition back to supersonic flow and indicates that the combustion process is isolated from the atmospheric back pressure.

While the pressures in the isolator and onset of the precombustion shock train are nearly the same regardless of fuel split ratio, pressures are noticeably different in the combustor section between the cavity and the thermal throat (from x/h = 5 to 35). Here the flow is subsonic in a one-dimensional sense and heat released in the flame drives the pressure down. Clearly, the cases with all the fuel delivered through the cavity-side injector bank result in an initially steeper drop in pressure in the vicinity of the cavity closeout ramp (at x/h = 5), perhaps due to more robust combustion in the vicinity of the cavity. However, the more uniformly mixed cases result in higher combustor pressures overall and presumably would generate more thrust.

The practical effects of differences in the combustor pressure can be quantified by calculating the integrated pressure force on the diverging wall of the combustor from x/h = 5.9 to 18.3. The integrated pressure force is related to integrated thrust, but neglects momentum and viscous drag. In this context it represents a metric for comparing engine performance related to pressure distributions in the diverging portion of the combustor flowpath. The combustor duct has a uniform width and a linear divergence on the cavity-side wall. Thus, the integrated pressure force is given by:

$$F = W \tan\theta \int_{x_1}^{x_2} p(x) dx \tag{5}$$

where $p(x)$ is the axial static pressure variation, W is the lateral width of the duct, and θ is the angle of divergence relative to the main axis of the duct. Integrated pressure forces for several different fueling scenarios and global equivalence ratios are shown in Fig. 9. The solid symbols represent cases with fuel injection from both the cavity-side and opposite-side fuel injectors while the open symbols represent cavity-side fueling only. The integrated pressure force with cavity-side only fueling is consistently on the order of 5% below the cases with fueling from both walls for all cases with a global equivalence ratio greater than 0.3. This means that there are potential thrust benefits in maximizing the fuel-air premixing, as opposed to a non-premixed or stratified fueling mode as seen in the present study with fuel injected from only one wall of the flowpath. Further, as seen in Figs. 7 and 8, this increase in combustor pressure from maximized fuel-air premixing does not change the pressure ratio or length of the precombustion shock train in the isolator. Thus, the increased potential thrust generation does not come with the expense of a longer isolator to contain the shock train. Note that there is very little change in the integrated pressure force as the equivalence ratio increases beyond 0.4. This is because the precombustion shock train cannot accommodate any additional pressure rise and the combustor pressures are essentially unchanged from those shown in Fig. 7. Continuing to increase the fuel rate from this point will quickly cause the isolator to unstart.

Since the effects on flame stability of injecting fuel upstream of the scramjet combustor are uncertain, an important aspect of these experiments was to determine the limits of operability of the flowpath. As mentioned above, the upper limit on equivalence ratio has been determined to be 0.45 to avoid impingement of the shock train on the upstream fuel injectors. In order to determine the lower flameholding limits, a number of lean and low temperature flameout tests were performed by slowly lowering either the fuel flow rate (lean flameout) or heater temperature (low temperature flameout) until the flame was no longer sustained. Figure 10 shows the results of these tests with each data point representing an observed flameout. Although there is some variability in the data, flameout consistently occurs at a global equivalence ratio just above 0.3 when the total temperature is 1200 K. Thus, the maximum range of equivalence ratio is about 0.14 or a little over 30% of the maximum equivalence ratio. At lower temperatures between 1000 K and 1100 K, the fuel equivalence ratio required to sustain combustion rises to between 0.35 and 0.39 resulting in a range of operability of only 0.06 or 13%. Additional tests were performed using the air throttle to provide additional back pressure such that the leading edge of the precombustion shock train was maintained at $x/h = -45$. At a total temperature of 1200 K, the incremental increase in static temperature behind the longer shock train sustains combustion down to an equivalence ratio between 0.26 and 0.29. This represents approximately 10% less fuel than with the air throttle off and gives an operability range in equivalence ratio of 0.16 to 0.19, which is between 35% and 45% of the maximum equivalence ratio. These results indicate that stable flameholding can be achieved over a range of conditions when operating the scramjet combustor in a premixed mode. Further, if the precombustion shock train backpressure is enhanced artificially, such as by using an air throttle, then the lean operability range can be extended.

Figure 11 is an instantaneous, high-speed chemiluminescence image taken at a global equivalence ratio of 0.41 with approximately 2/3 of the fuel from the cavity-side injector bank and 1/3 from the opposite-side bank. The dotted white lines represent the limits of the duct with the cavity flameholder at the bottom Figure 12 is the same image taken at a global equivalence ratio of 0.31. The chemiluminescence is primarily due to emission from excited CH in the active reaction zone. Both images were taken with a 0.6 ms exposure. At both equivalence ratios, the flame is anchored on the cavity with combustion initiating along the shear layer between the cavity and the freestream air, impinges on the sloped cavity closeout surface, and propagates downstream expanding away from the cavity-side wall with an angle relative to the wall of approximately 11.5° in Fig. 11 and 9.5° in Fig. 12. There is little to no chemiluminescence near the cavity leading edge in either case. As would be expected, the higher fuel rate results in a somewhat more robust and brighter flame. The field of view is limited to 6.6 cavity depths (59.69 mm) downstream of the cavity leading edge and at that point the flame propagates a little over halfway across the duct in Fig. 11 and a little less than halfway in Fig. 12. These and other images demonstrated that the flame was anchored on the cavity flameholder.

IV. Conclusion

This paper documents the development of a dual-mode scramjet flowpath and fuel injection scheme that is capable of sustaining a high-speed, uniformly premixed, turbulent flame with

a combustor inlet Mach number of about 0.7. This is the first time in the literature that a dual-mode scramjet has been operated using fully premixed combustion. The continuous, long-duration, and stable nature of the scramjet flame described here presents an opportunity for the application of advanced diagnostic measurement techniques to more fully explore the combustion process that is central to these engines. Such diagnostics include fine-grid CARS as well as PLIF and PIV, which can be performed in sufficient quantity to yield statistically meaningful quantitative results. The mode of operation relies on a precombustion shock train in the isolator to enhance the fuel-air mixing. The resulting fuel-air premix uniformity at the leading edge of the cavity flameholder has been verified with NO PLIF. Static wall pressures are presented along with lean and low-temperature flameout data, integrated pressure forces, and chemiluminescence images.

Within the operability limits of the flowpath documented in this paper, the scramjet flame is stably anchored on the cavity and is highly repeatable. The fully premixed cases produce a 5% greater integrated pressure force in the combustor when compared with more stratified fueling scenarios indicating the potential for increased thrust capacity in that case. This difference may be greater with the addition of a thrust nozzle and exhaust to vacuum rather than the atmospheric back pressure of the laboratory in the present experiment. Further, the increased pressure force is not associated with an increase in the length of the precombustion shock train. This suggests improved combustor performance without the need to lengthen the isolator.

Acknowledgments

This research was sponsored by the National Center for Hypersonic Combined Cycle Propulsion grant FA 9550-09-1-0611. The technical monitors on the grant are Chiping Li (AFOSR) and Aaron Auslender and Rick Gaffney (NASA).

References

[1]. Peters N, Turbulent Combustion, Cambridge University Press, 2000.

[2]. Borghi R, “Turbulent Combustion Modeling,” Progress in Energy and Combustion Science, Vol. 14, No. 4, 1988, pp. 245292.

[3]. Bray K, Libby P, and Williams F, High-Speed Turbulent Combustion in Turbulent Reacting Flows (eds. Libby PA and Williams FA), Academic Press, London, UK, 1994.

[4]. Williams FA, Combustion Theory, Westview Press, 1985.

[5]. Ben-Yakar A and Hanson RK, “ Cavity Flame-Holders for Ignition and Flame Stabilization in Scramjets: An Overview,” Journal of Propulsion and Power, Vol. 17, No. 4, 2001, pp. 869–877.

[6]. Gruber MR, Baurle RA, Mathur T, and Hsu KY, “Fundamental Studies of Cavity-Based Flameholder Concepts for Supersonic Combustors,” Journal of Propulsion and Power, Vol. 17, No. 1, 2001, pp.146–153.

[7]. Mathur T, Gruber M, Jackson K, Donbar J, Donaldson W, Jackson T, and Billig F, “Supersonic Combustion Experiments with a Cavity-Based Fuel Injector,” Journal of Propulsion and Power, Vol. 17, No. 6, 2001, pp. 1305–1312.

[8]. Gruber MR, Donbar JM, Carter CD, and Hsu KY, “Mixing and Combustion Studies Using Cavity-Based Flameholders in a Supersonic Flow,” Journal of Propulsion and Power, Vol. 20, No. 5, 2004, pp.769–778.

[9]. Milligan RT, Liu J, Tam CJ, Eklund DR, Hagenmaier MA, Davis DL, Risha DJ, Gruber M, and Mathur T, “Dual-Mode Scramjet Combustor: Numerical Sensitivity and Evaluation of Experiments,” AIAA Paper 2012–0947, 2012.

[10]. Tatman BJ, Rockwell RD, Goyne CP, McDaniel JC, and Donohue JM, “Experimental Study of Vitiation Effects on Flameholding in a Cavity Flameholder,” Journal of Propulsion and Power, Vol. 29, No. 2, 2013, pp. 417–423.

[11]. Henry JR and Anderson GY, “Design Considerations for the Airframe-Integrated Scramjet,” NASA Report No. TM X2895, 1973.

[12]. Menon S, “Shock-Wave-Induced Mixing Enhancement in Scramjet Combustors,” AIAA Paper 89–0104, 1989.

[13]. Wood CW and Schetz JA, “Effects of Unsteady Shock Impingement on High-Speed Gaseous Mixing,” AIAA Paper 91-5091, 1991.

[14]. Victor KG, “Influence of Back-Pressure-Induced Shock Systems on Transverse Jet Mixing with a Mach 2.9 Freestream,” Master’s Thesis, Engineering Physics Dept., Univ. of Virginia, Charlottesville, VA, 1994.

[15]. Choi B, Takae K, Kouchi T, and Masuya G, “Turbulent Characteristics for Jet Injected into Supersonic Flow with Pseudo Shock Wave,” Journal of Propulsion and Power, Vol. 28, No. 5, 2012, pp. 971–981.

[16]. Vasiliev V, Zakotenko SN, Krasheninnikov SY, and Stepanov VA, “Numerical Investigation of Mixing and Augmentation Behind Oblique Shock Waves,” AIAA Journal, Vol. 32, No. 2, 1994, pp. 311–316.

[17]. Vinogradov VA, Shikhman YM, and Segal C, “A Review of Fuel Pre-Injection in Supersonic, Chemically Reacting Flows,” Applied Mechanics Reviews, Vol. 60, No. 4, 2007, pp. 139–148.

[18]. Heiser WH and Pratt DT, Hypersonic Airbreathing Propulsion, AIAA Education Series, AIAA, Washington, D.C., 1994, pp. 305–306.

[19]. Lee SH, Characteristics of Dual Transverse Injection in Scramjet Combustor, Part 1: Mixing,” Journal of Propulsion and Power, “ Vol. 22, No. 5, 2006, pp. 1012–1019.

[20]. Livingston T, Segal C, Schindler M, and Vinogradov VA, “Penetration and Spreading of Liquid Jets in an ExternalInternal Compression Inlet,” AIAA Journal, Vol. 38, No. 6, 2000, pp. 989–994.

[21]. Owens M, Mullagiri S, Segal C, and Vinogradov VA, “Effects of Fuel Preinjection on Mixing in Mach 1.6 Airflow,” Journal of Propulsion and Power, Vol. 17, No. 3, 2001, pp.605–610.

[22]. Lee SH and Mitani T, “Mixing Augmentation of Transverse Injection in Scramjet Combustor,” Journal of Propulsion and Power, Vol. 19, No. 1, 2003, pp. 115–124.

[23]. Gruber MR, Carter CD, Montes DR, Haubelt LC, King PI, and Hsu KY, “Experimental Studies of Pylon-Aided Fuel Injection into a Supersonic Crossflow,” Journal of Propulsion and Power, Vol. 24, No. 3, 2008, pp. 460–470.

[24]. Rowan SA and Paull A, “Performance of a Scramjet Combustor with Combined Normal and Tangential Fuel Injection,” Journal of Propulsion and Power, Vol. 22, No. 6, 2006, pp. 1334–1338.

[25]. Gardner AD, Paull A, and McIntyre TJ, “Upstream Porthole Injection in a 2-D Scramjet Model,” Shock Waves, Vol. 11, No. 5, 2002, pp. 369–375.

[26]. McGuire JR, Boyce RR, and Mudford NR, “Radical farm ignition processes in two-dimensional supersonic combustion,” Journal of Propulsion and Power, Vol. 24, No. 5, 2008, pp. 1248–1257.

[27]. Boyce RR, Mudford NR, and McGuire JR, “OH-PLIF visualization of radical farming supersonic combustion flows,” Shock Waves, Vol. 22, No. 1, 2012, pp. 9–21.

[28]. Haas JF and Sturtevant B, “Interaction of Weak Shock Waves with Cylindrical and Spherical Gas Inhomogeneities,” Journal of Fluid Mechanics, Vol. 181, 1987, pp. 41–76.

[29]. Hermanson JC and Cetegen BM, “Shock-Induced Mixing of Nonhomogeneous Density Turbulent Jets,” Physics of Fluids, Vol. 12, No. 5, 2000, pp. 1210–1225.

[30]. Nedungadi A, and Lewis MJ, “Numerical Study of Fuel Mixing Enhancement Using an Oblique Shock/Vortex Interaction,” Journal of Propulsion and Power, Vol. 16, No. 6, 2000, pp. 946–955.

[31]. Marble FE, Zukoski EE, Jacobs JW, Hendricks GJ, and Waitz IA, “Shock Enhancement and Control of Hypersonic Mixing and Combustion,” AIAA Paper 90–1981, 1990.

[32]. Waitz IA, Marble FE, and Zukoski EE, “Investigation of a Contoured Wall Injector for Hypervelocity Mixing Augmentation,” AIAA Journal, Vol. 31, No. 6, 1993, pp. 1014–1021.

[33]. Yang J, Kubota T, and Zukoski EE, “Applications of Shock-Induced Mixing to Supersonic Combustion,” AIAA Journal, Vol. 31, No. 5, 1993, pp. 854–862.

[34]. Cutler AD, Magnotti G, Cantu L, Gallo E, Rockwell RD, and Goyne CP, “Dual-Pump Coherent Anti-Stokes Raman Spectroscopy Measurements in a Dual-Mode Scramjet,” Journal of Propulsion and Power, Vol. 30, No. 3, 2014, pp. 539–549.

[35]. Johansen CT, McRae CD, Danehy PM, Gallo EC, Cantu LM, Magnotti G, Cutler AD, Rockwell RD, Goyne CP, and McDaniel JC, “OH PLIF of UVa Supersonic Combustion Experiment: Configuration A,” Journal of Visualization, Vol. 17, No. 2, 2014, pp. 131–141.

[36]. Rice BE, Goyne CP, McDaniel JC, and Rockwell RD, “Characterization of a Dual-Mode Scramjet via Stereoscopic Particle Image Velocimetry,” AIAA 2014–0986, 52nd AIAA Aerospace Sciences Meeting, National Harbor, MD, 1 2014.

[37]. Fulton JA, Edwards JR, Hassan HA, McDaniel JC, Goyne CP, Rockwell RD, Cutler AD, Johansen CT, and Danehy PM, “Large-Eddy/Reynolds-Averaged Navier-Stokes Simulations of Reactive Flow in Dual-Mode Scramjet Combustor,” Journal of Propulsion and Power, Vol. 30, No. 3, 2014, pp. 558–575.

[38]. Rockwell RD, Goyne CP, Rice BE, Kouchi T, McDaniel JC, and Edwards JR, “Collaborative Experimental and Computational Study of a Dual-Mode Scramjet Combustor,” Journal of Propulsion and Power, Vol. 30, No. 3, 2014, pp. 530538.

[39]. Ullum U, Schmidt JJ, Larsen PS, and McCluskey DR, “Statistical Analysis and Accuracy of PIV Data,” Journal of Visualization, Vol. 1, No. 2, 1998, pp. 205–216.

[40]. Cantu LM, Gallo EC, Cutler AD, Bathel BF, Danehy PM, Rockwell RD, Goyne CP, and McDaniel JC, “Visualization of Simulated Fuel-Air Mixing in a Dual-Mode Scramjet,” Journal of Propulsion and Power, Vol. 32, No. 2, 2016, pp. 373–382.

[41]. Rockwell RD, Goyne CP, Haw W, Krauss RH, McDaniel JC, and Trefny CJ, “Experimental Study of TestMedium Vitiation Effects on Dual-Mode Scramjet Performance and Power,” Journal of Propulsion and Power, Vol.27, No.5, 2011, pp. 1135–1142.

[42]. Krauss RH, McDaniel JC, Scott JE, Whitehurst RB, Segal C, Mahoney GT, and Childers JM, “Unique, clean-air, continuous-flow, high-stagnation-temperature facility for supersonic combustion research,” AIAA Paper 88–3059, 1988.

[43]. Krauss RH and McDaniel JC, “A Clean Air Continuous Flow Propulsion Facility,” AIAA Paper 92–3912, 1992.

[44]. Ramesh K, Edwards JR, Chelliah H, Goyne C, McDaniel J, Rockwell R Kirik J, Cutler A, and Danehy P, “Large Eddy Simulation of High-Speed, Premixed Ethylene Cumbustion,” AIAA 2015–0356, 53rd AIAA Aerospace Sciences Meeting, Kissimmee, FL, 1 2015.

[45]. Cutler AD, Cantu LML, Gallo ECA, Baurle R, Danehy PM, Rockwell RD, Goyne CP, and McDaniel JC, “Nonequilibrium Supersonic Freestream Studied Using Coherent Anti-Stokes Raman Spectroscopy,” AIAA Journal, Vol. 53, No. 9, 2015, pp. 2762–2770.

[46. Gallo ECA, Cantu LML, Cutler AD, Rockwell RD, Goyne CP, and McDaniel JC, “WIDECARS Measurements of a Premixed Ethylene-Air Flame in a Small-Scale Dual-Mode Scramjet Combustor,” AIAA 2016–0656, 54rh AIAA Aerospace Sciences Meeting, San Diego, CA, 1 2016.

[47]. Cutler AD, Gallo ECA, Cantu LML, Rockwell RD, and Goyne CP, “WIDECARS Measurements of the Turbulent, Premixed Ethylene-Air Flame in a Dual-Mode Scramjet,” AIAA 2016–3111, 32nd AIAA Aerodynamic Measurement Technology and Ground Testing Conference, Washington, D.C., 6 2016.

[48]. Cantu LML, Gallo ECA, Cutler AD, Danehy PM, Johansen CT, Rockwell RD, Goyne CP, and McDaniel JC, “OH-PLIF Visualization of a Premixed Ethylene-Fueled Dual-Mode Scramjet Combustor,” AIAA 2016–1763, 54th AIAA Aerospace Sciences Meeting, San Diego, CA, 1 2016.

[49]. Heiser WH and Pratt DT, Hypersonic Airbreathing Propulsion, AIAA Education Series, AIAA, Washington, D.C., 1994, pp. 332–346.

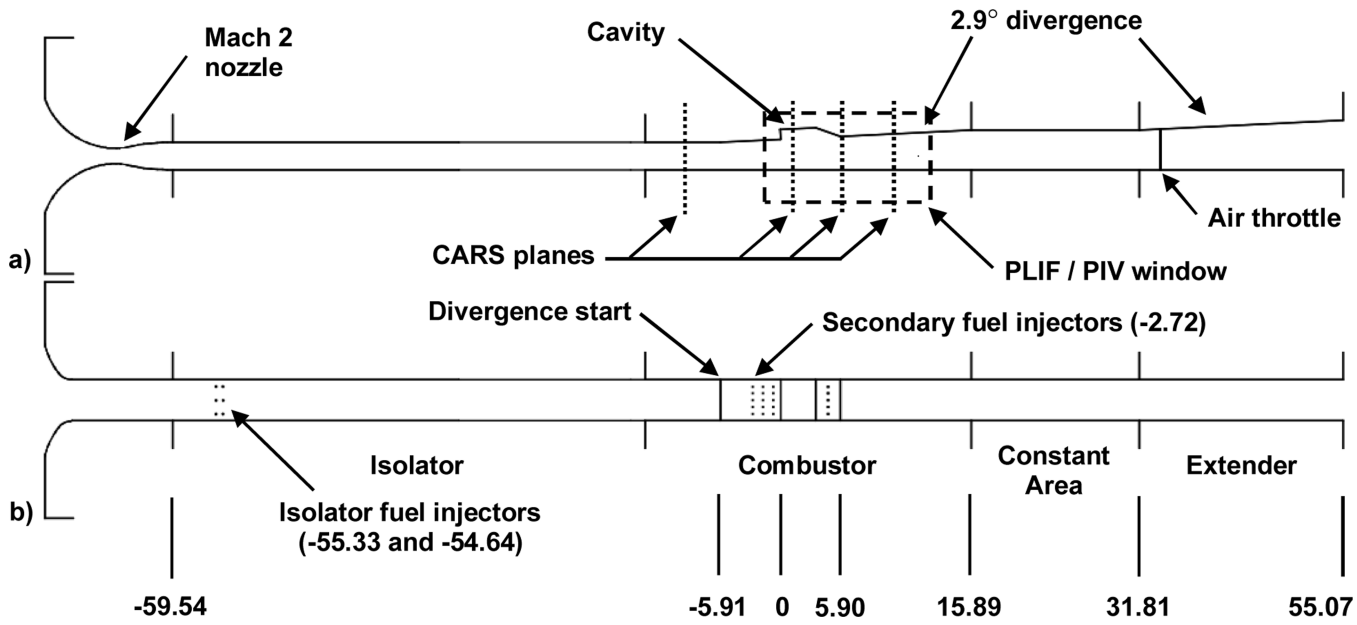

Figure 1.

Modified Configuration E flowpath: a) side view and b) top view with axial distances from cavity leading edge normalized by cavity depth (h = 9.04 mm).

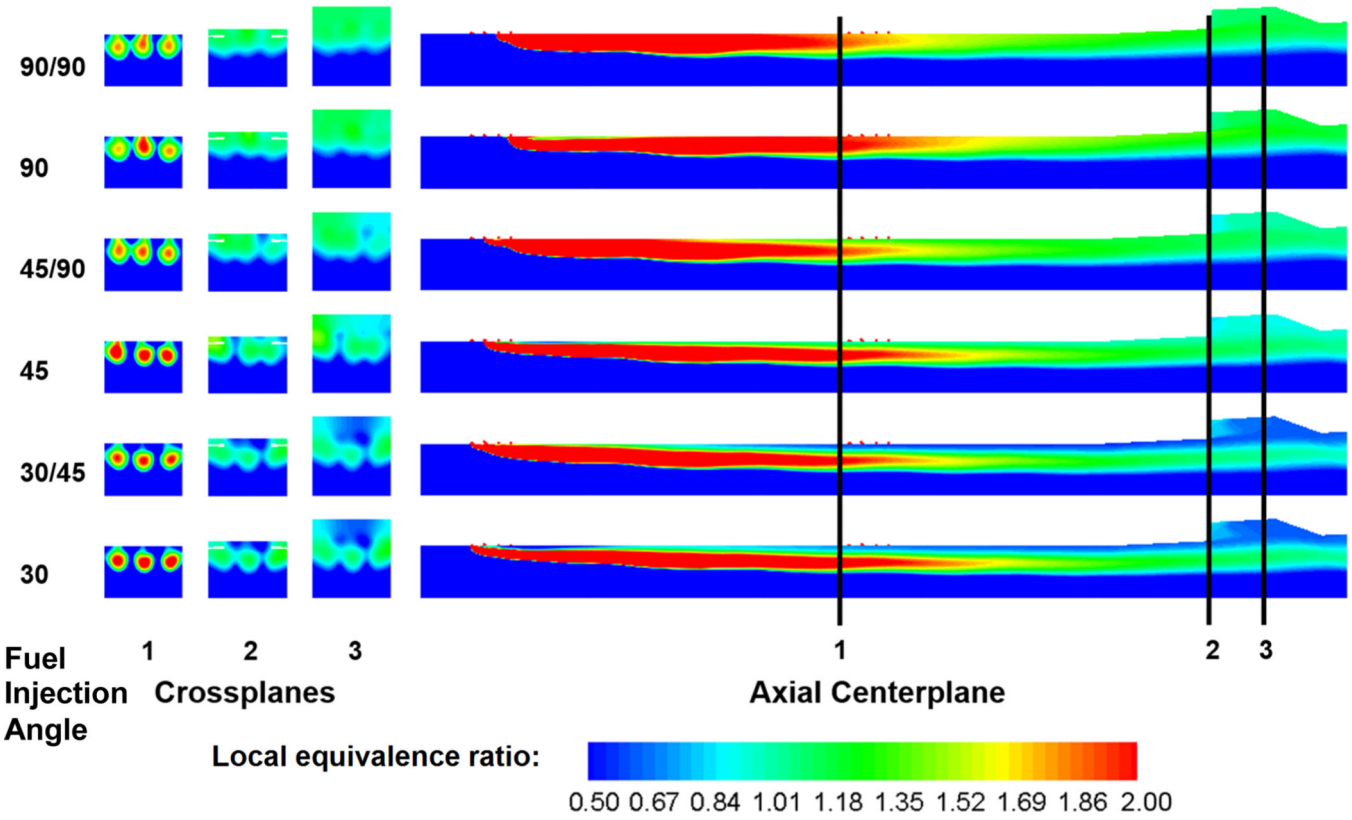

Figure 2.

RANS CFD results for several potential non-backpressured mixing strategies showing local equivalence ratio in the isolator and cavity, global equivalence ratio = 0.5.

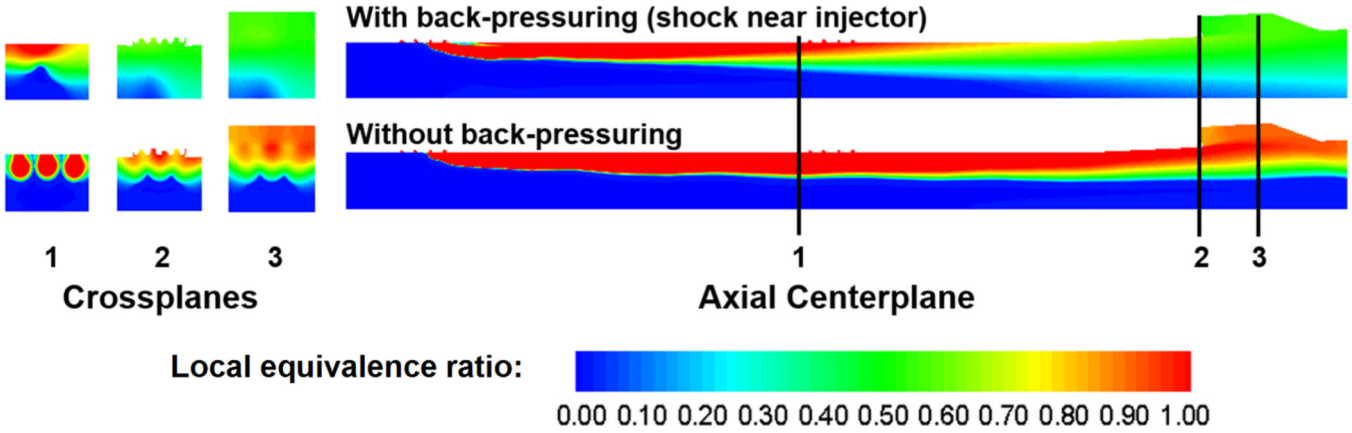

Figure 3.
RANS CFD results showing the effect of an isolator shock train on the local equivalence ratio in the isolator and cavity, global equivalence ratio = 0.35.

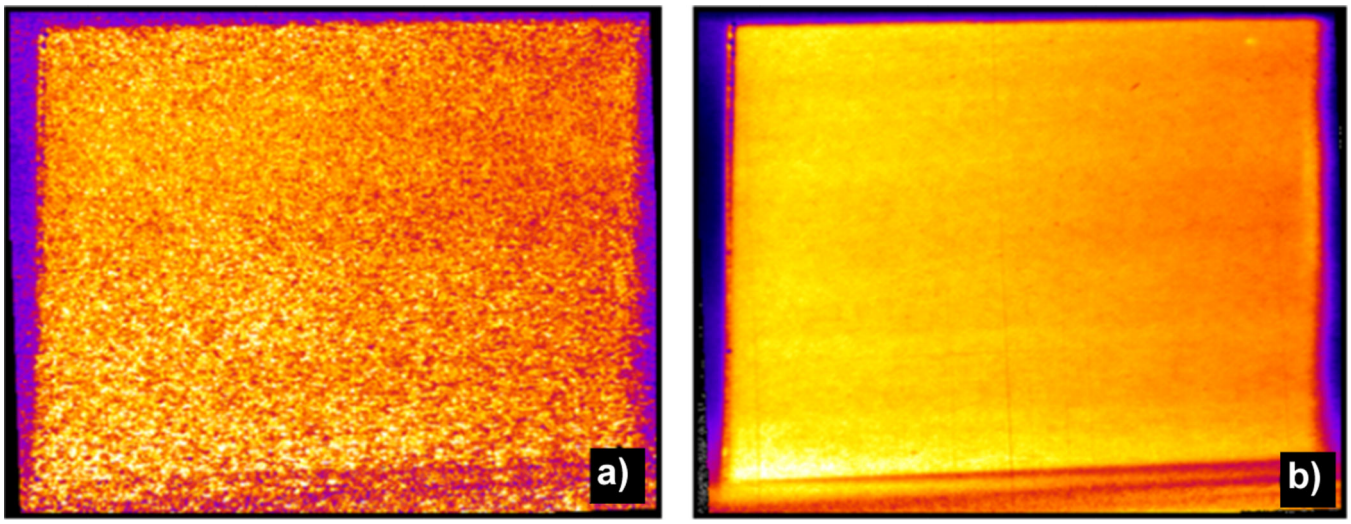

Figure 4:

Instantaneous (a) and averaged (b) NO PLIF images of fuel simulant distribution at the cavilty leading edge for two rows of fuel injection from both walls with global equivalence ratio = 0.44 and shock train leading edge at x/h = −45 (adapted from [40]).

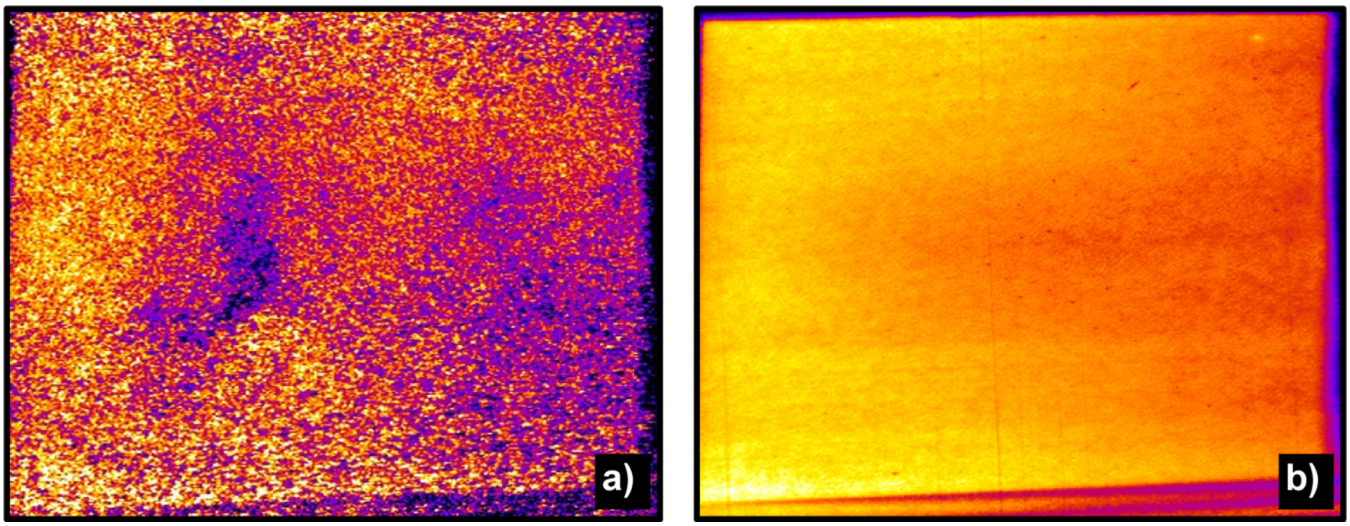

Figure 5.

Instantaneous (a) and averaged (b) NO PLIF images of fuel simulant distribution at the cavity leading edge for two rows of fuel injection from both walls with global equivalence ratio = 0.35 and shock train leading edge at x/h = −30 (adapted from [40]).

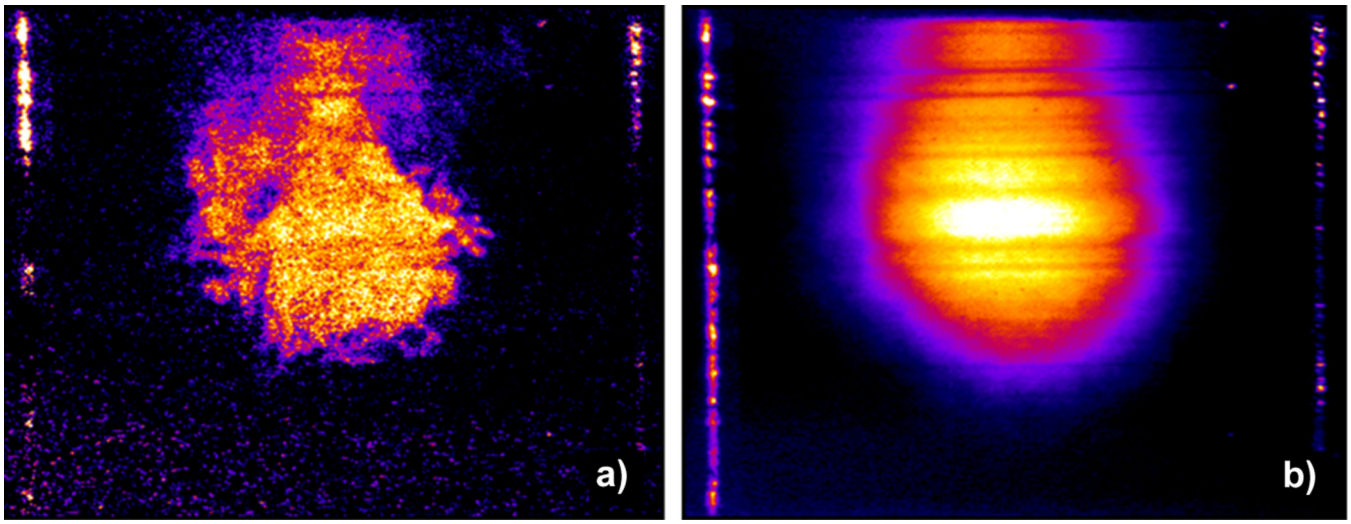

Figure 6:
Instantaneous (a) and averaged (b) NO PLIF images of fuel simulant distributions for a single fuel injector with equivalence ratio = 0.09 and no shock train (adapted from [40]).

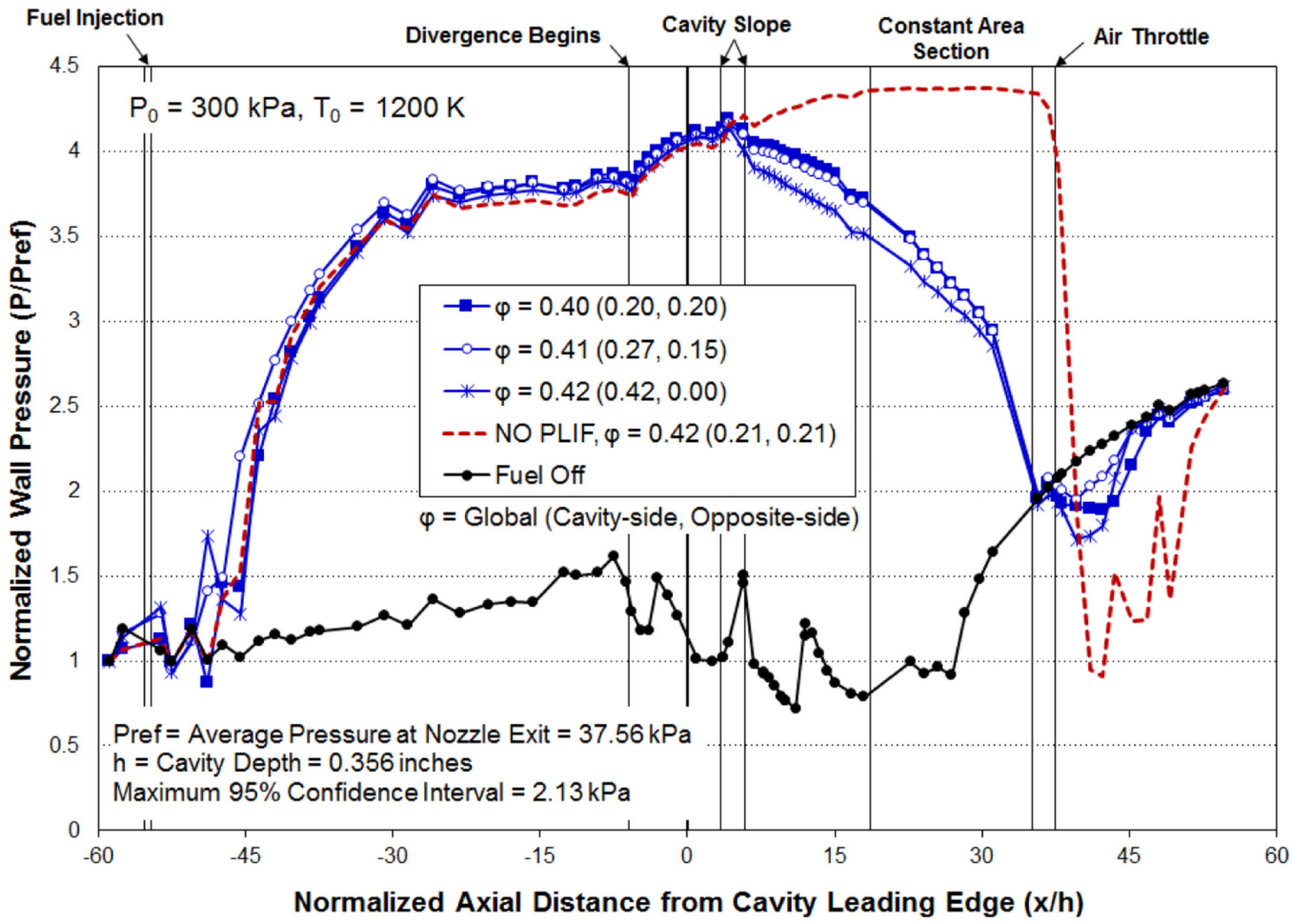

Figure 7.

Normalized wall pressures at fuel condition 1. In the legend, the numbers in parentheses indicate the cavity-side and opposite-side fuel equivalence ratio, respectively.

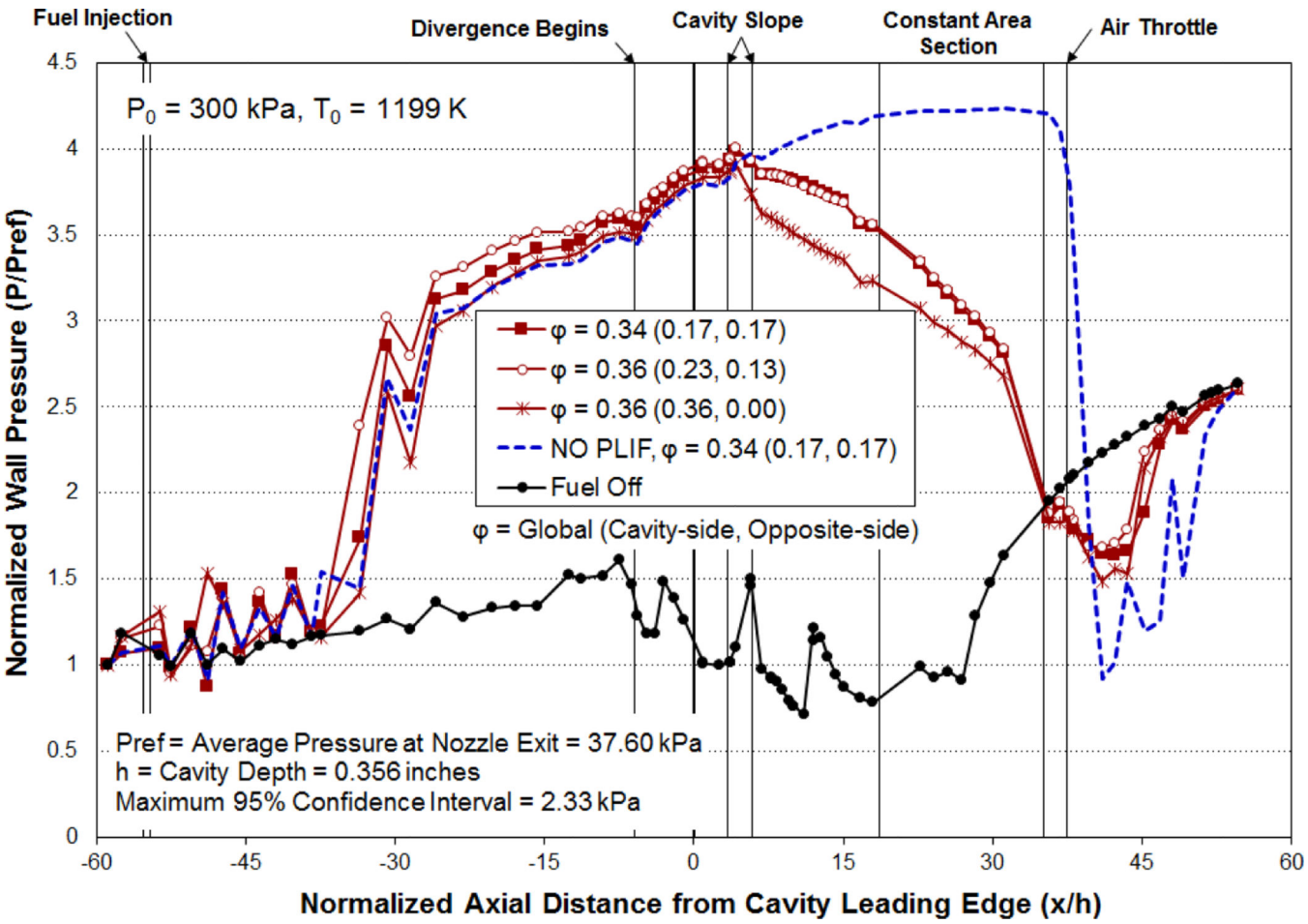

Figure 8.

Normalized wall pressures at fuel condition 2. In the legend, the numbers in parentheses indicate the cavity-side and opposite-side fuel equivalence ratio, respectively.

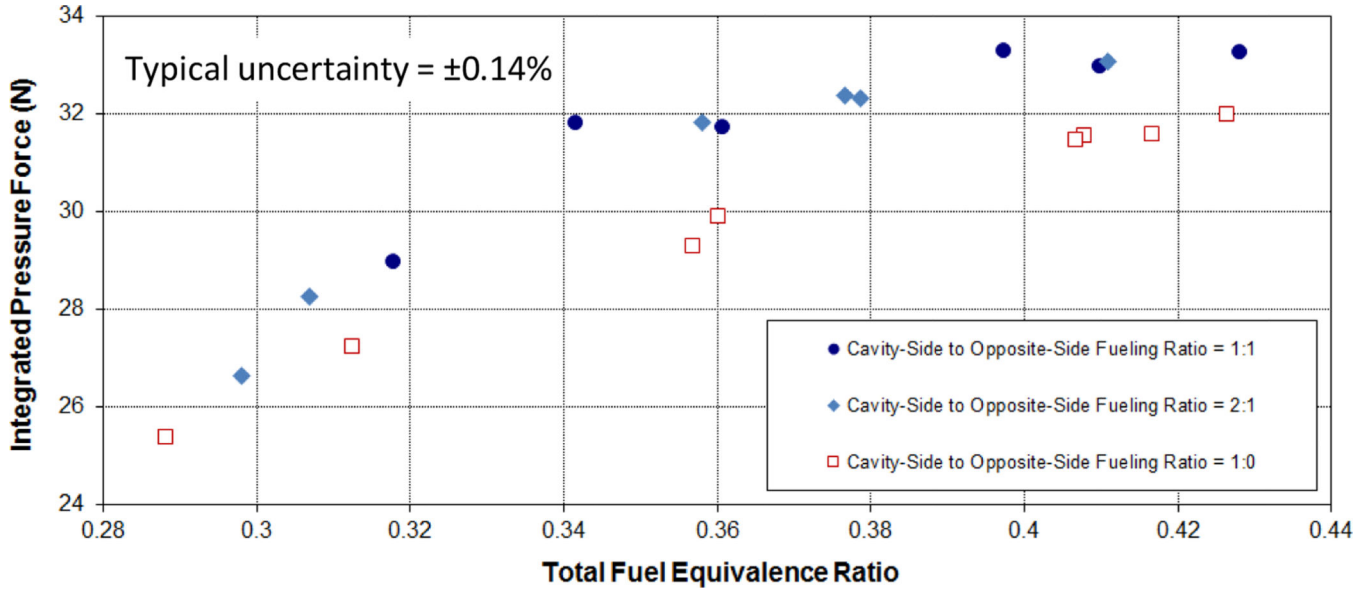

Figure 9.
Integrated pressure force as a function of global fuel equivalence ratio.

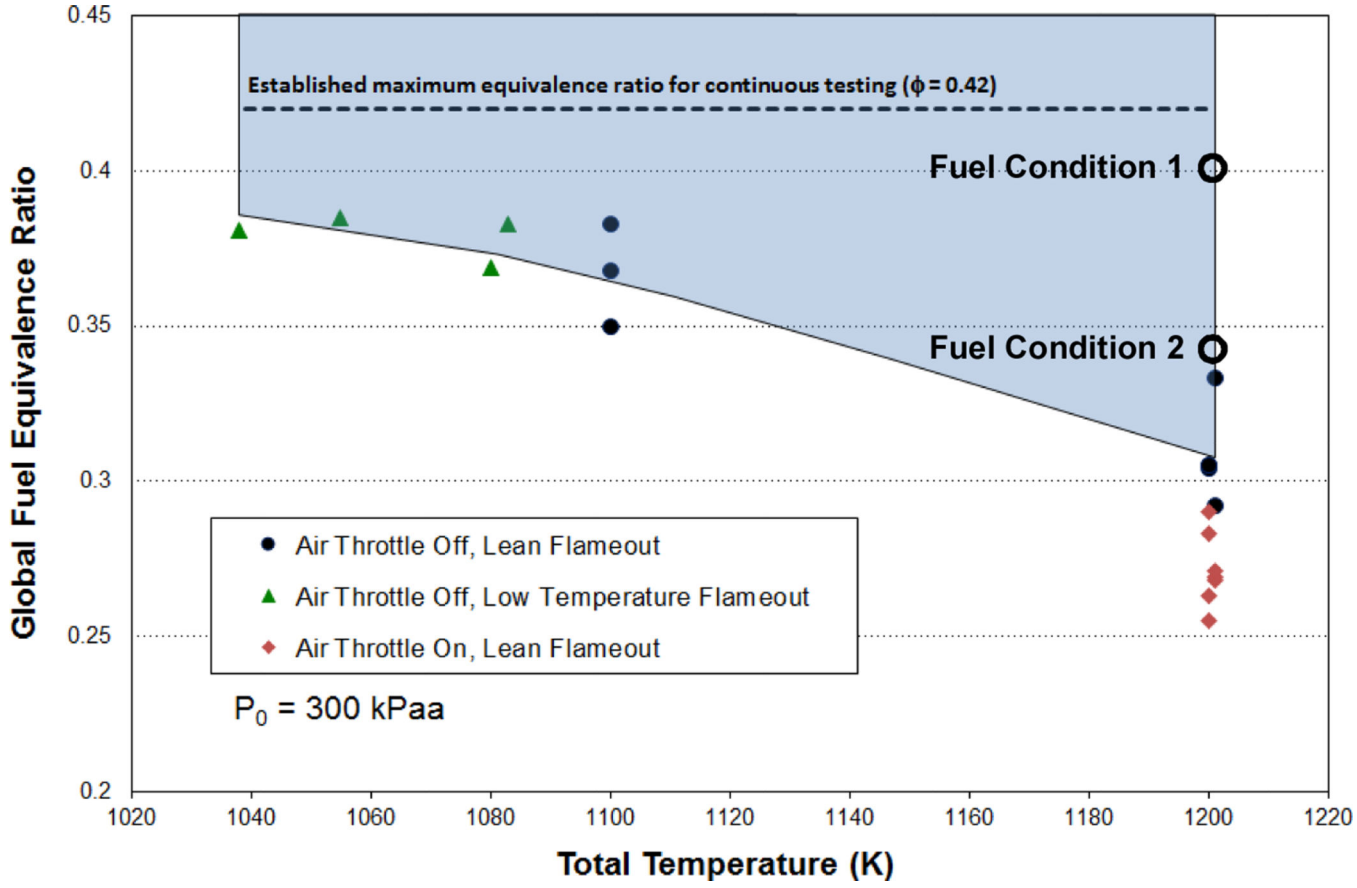

Figure 10.

Lean and low temperature flameout points. Shaded area represents the region of stable combustion in the facility. Fuel conditions 1 and 2, from Table 3, are shown for reference.

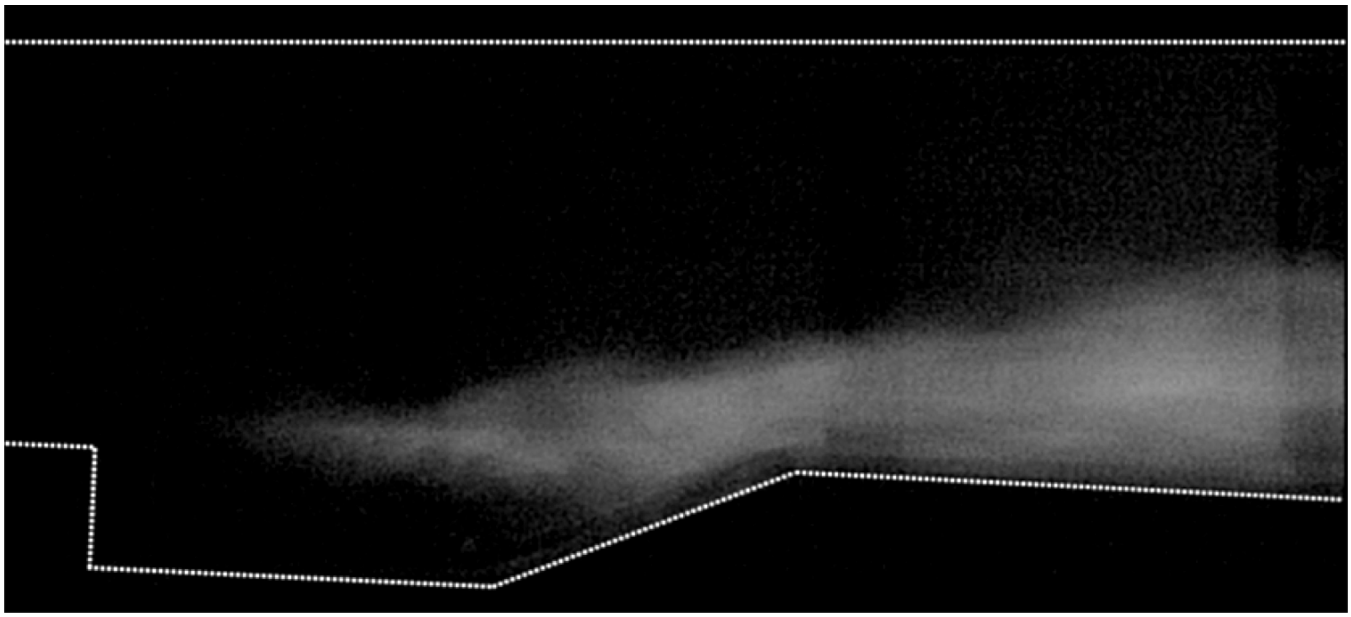

Figure 11.
Chemiluminescence image (0.6 ms capture) at global $\varphi = 0.41$ (cavity-side = 0.27, opposite-side = 0.15).

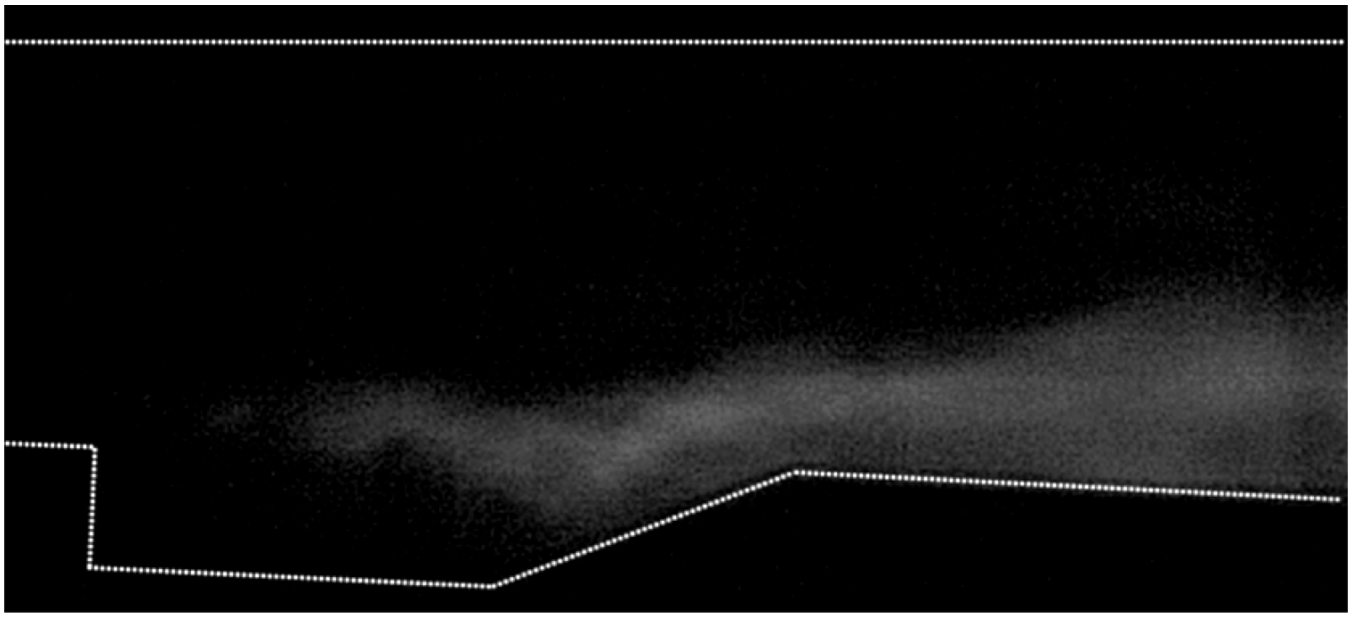

Figure 12.
Chemiluminescence image (0.6 ms capture) at global $\varphi = 0.31$ (cavity-side = 0.20, opposite-side = 0.11).

Table 1.

Test conditions for main air flow.

Parameter	Air	Uncertainty
Total pressure (kPa)	300	± 1%
Total temperature (K)	1200	± 0.8%
Mass flow rate (g/s)	185.9	± 1.7%
Mach number *	2.04	± 1%

* Property at nozzle exit determined using nozzle area ratio and assuming isentropic flow (γ=1.36 for air).

Table 2.

Potential ethylene fuel injection configurations and dynamic pressures for the UVASCF.

	Number of		Each Jet	
Global φ	**Rows**	**Jets**	**Q (kPa)**	**Q ratio**
0.17	1	3	149.79	1.42
	2	6	74.90	0.71
	3	9	49.93	0.47
	4	12	37.45	0.36
0.20	1	3	176.22	1.17
	2	6	88.11	0.83
	3	9	58.74	0.56
	4	12	44.06	0.42
0.50	1	3	440.55	4.17
	2	6	220.28	2.09
	3	9	146.85	1.39
	4	12	110.14	1.04

Note: Table assumes injection upstream of the precombustion shock train and all jets are identical with a discharge coefficient per row of 0.60 (γ=1.36 for air, 1.24 for C_2H_4). Shaded rows indicate configurations used for the experiments described in this paper.

Table 3.

Test conditions for ethylene fuel.

Parameter	Fuel Condition 1		Fuel Condition 2		Uncertainty
	Cavity-Side	Opposite-Side	Cavity-Side	Opposite-Side	
Equivalence ratio	0.20	0.20	0.17	0.17	± 3.7%
Total pressure (kPa)	256	271	220	229	± 2.3%
Total temperature (K)	289	289	286	286	± 1.9%
Mach number *	1.0	1.0	1.0	1.0	± 0.5%

* Property at nozzle exit determined using nozzle area ratios and assuming isentropic flow (γ=1.36 for air, 1.24 for C_2H_4).